FTIR Study of CO_2 and H_2O/CO_2 Nanoparticles and Their Temporal Evolution at 80 K

M. Taraschewski,[†,‡] H. K. Cammenga,[†] R. Tuckermann,[‡] and S. Bauerecker*[,†,‡]

Institut für Physikalische und Theoretische Chemie, Technische Universität Braunschweig, Hans-Sommer-Strasse 10, D-38106 Braunschweig, Germany, and Institut für Küstenforschung/Physikalische und Chemische Analytik, GKSS-Forschungszentrum GmbH, Max-Planck-Strasse 1, D-21502 Geesthacht, Germany

Received: December 29, 2004; In Final Form: February 15, 2005

Fourier transform infrared (FTIR) spectroscopy combined with a long-path collisional cooling cell was used to investigate the temporal evolution of CO_2 nanoparticles and binary H_2O/CO_2 nanocomposites in the aerosol phase at 80 K. The experimental conditions for the formation of different CO_2 particle shapes as slab, shell, sphere, cube, and needle have been studied by comparison with calculated data from the literature. The H_2O/CO_2 nanoparticles were generated with a newly developed multiple-pulse injection technique and with the simpler flow-in technique. The carbon dioxide ν_3-vibration band at 2360 cm^{-1} and the water ice OH-dangling band at 3700 cm^{-1} were used to study the evolution of structure, shape, and contact area of the nanocomposites over 150 s. Different stages of binary nanocomposites with primary water ice cores were identified dependent on the injected CO_2 portion: (a) disordered (amorphous) CO_2 slabs on water particle surfaces, (b) globular crystalline CO_2 humps sticking on the water cores, and (c) water cores being completely enclosed in bigger predominantly crystalline CO_2 nanoparticles. However, regular CO_2 shell structures on primary water particles showing both longitudinal (LO) and transverse (TO) optical mode features of the ν_3-vibration band could not be observed. Experiments with reversed nucleation order indicate that H_2O/CO_2 composite particles with different initial structures evolve toward similar molecular nanocomposites with separated CO_2 and H_2O regions.

I. Introduction

The binary system of water and carbon dioxide is of importance in different research topics as biochemical, atmospheric, extraterrestrial, or technical systems. For example, typical interstellar ice consists of a polar (mostly water) and a nonpolar (often carbon monoxide or carbon dioxide) phase.[1] The nanoparticles compounded of both components could serve as a model system for interactions of carbon dioxide with relatively large ice surfaces. While theoretical studies on binary water/carbon dioxide complexes are scarce,[2,3] experimental investigations have been performed on carbon-dioxide clathrate hydrates as surface deposits with films[4,5] and nanocrystals supported on infrared windows[6] at about 120 K. Yet up to now, experimental investigations on composite water/carbon dioxide nanoparticles suspended in the aerosol phase have not been carried out to our knowledge.

Recently, we have developed a new technique for the generation of multilayered molecular nanoparticles and have observed self-diffusion in core-shell composite $^{12}CO_2/^{13}CO_2$ nanoparticles.[7] In the present work, this multiple-pulse sample-gas inlet technique and other techniques have been applied to the generation of binary H_2O/CO_2 and CO_2/H_2O nanoparticles. This initial study will mainly focus (a) on the evidence that the CO_2 and H_2O molecules form composite (and not homogeneous) nanoparticles, (b) on the structure and shape of the nanocomposites, and (c) on their temporal evolution.

We start our presentation with some results of the temporal evolution of pure CO_2 nanoparticles to visualize the spectroscopic distinction to the composite H_2O/CO_2 nanoparticles. Although CO_2 nanoparticles are well-studied van der Waals-bonded systems under different aspects[8−15] as optical properties, particle structure, and shape, there exists only a little information on processes of the particles as shape evolution, phase transitions, and self-diffusion.[7] Combined with a 20-m White-cell cooling device, our system is sensitive enough to resolve such processes in the time scale of seconds and minutes.

Some of the spectroscopically relevant facts of CO_2 nanoparticles formed by collisional cooling are summarized: The size is manageable between 1 nm and 1 μm (10^2 and 10^{11} molecules per particle), predominantly by variation of sample gas concentration and buffer-gas temperature;[12] the structure is crystalline face-centered cubic ($Pa3$)[15,16,35−37] for generation temperatures above 50 K;[21] the cubic structure even builds up easily at small sizes of about 10^2 molecules per particle;[38] the amorphous phase can be reached and kept at temperatures below approximately 30 K;[11,17,21] at least smaller particles ($<10^3$ molecules per particle) are comparable to those generated in supersonic jet expansions.[17] The discussion of particle size and shape follows in section IIIA.

II. Experimental Section

The nanoparticles were formed in a long-path collisional cooling cell, which is described in detail by Bauerecker et al.[12] The experimental setup is schematically shown in Figure 1. In the present investigation, the cooling cell was operated in the stationary mode; that is, no buffer-gas flow was used. The infrared spectra were recorded with a Nicolet Magna 550 FTIR spectrometer equipped with a Globar light source, a KBr beam splitter, KBr windows, and an external InSb detector. The f/16 White optics, integrated in the cell, allows maximum absorption

* Corresponding author. E-mail: s.bauerecker@tu-bs.de.
† Technische Universität Braunschweig.
‡ GKSS-Forschungszentrum GmbH.

10.1021/jp044075r CCC: $30.25
Published on Web 03/30/2005

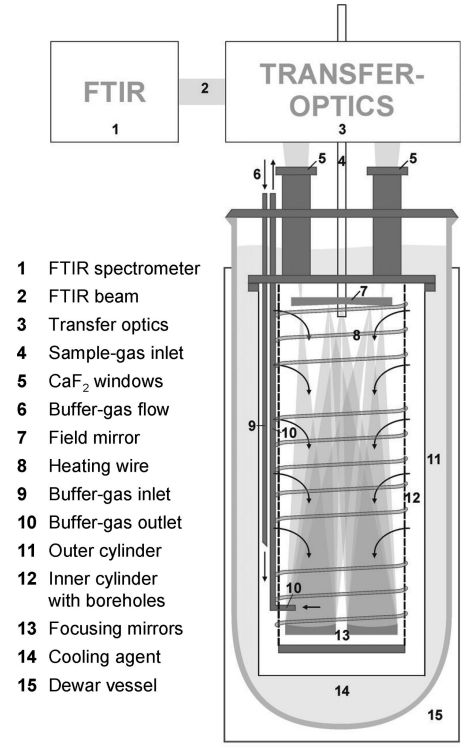

Figure 1. Experimental setup (schematic). For scale: the distance between field mirror (7) and focusing mirrors (13) is 0.625 m.

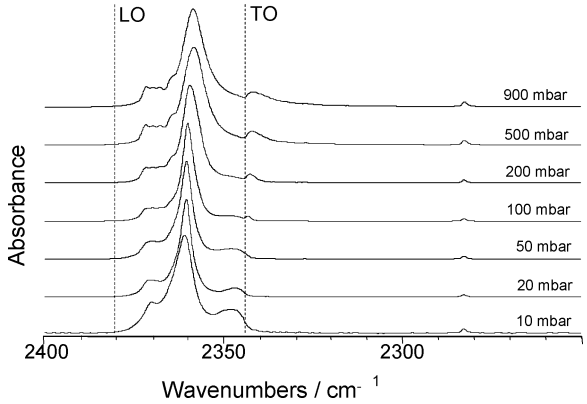

Figure 2. The ν_3-vibration band of CO_2 nanoparticles at 83 K at different sample gas pressures. The sample gas, 91 ppm CO_2 in He, was filled into the empty cell up to the target pressure for each spectrum.

path lengths up to 20 m. Temperatures can be adjusted between 4 and 400 K, but in this study we focused on temperatures of approximately 80 K. All spectra were recorded with an optical resolution of 1 cm^{-1}, a zero filling level of two, and Happ-Genzel apodization. The optical path length was 2.5 m (Figures 2 and 5) and 12.5 m (Figures 4, 6, and 7). The sampling time per spectrum was 120 s (Figures 2 and 4), 3.8 s (Figure 5), and 6.4 s (Figures 6 and 7). In Figures 2, 4, 5, 6, and 7, the spectra are scaled to the bottom spectrum. A number of further spectra, measured within the time series, are not shown for clarity.

Several sample-gas inlet techniques were used in this work. First, the sample gas was introduced as a laminar flow via mass-flow controllers (for results, see Figures 2 and 6). Here, the sample-gas inlet was stopped at the final pressure. Second, the sample gases were injected by separate pressure pulses using magnetic valves and a pulse generator that controls duration, repetition frequency, and phase differences of the single pulses. Here, the single gases were injected through the same inlet tube (and therefore being premixed in case of several components)

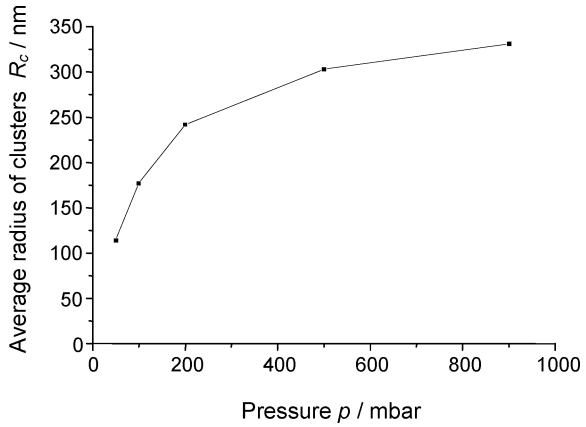

Figure 3. Average cluster radius in relation to the sample gas pressure computed from Mie theory using an adapted algorithm; compare text. For sampling conditions, see Figure 2.

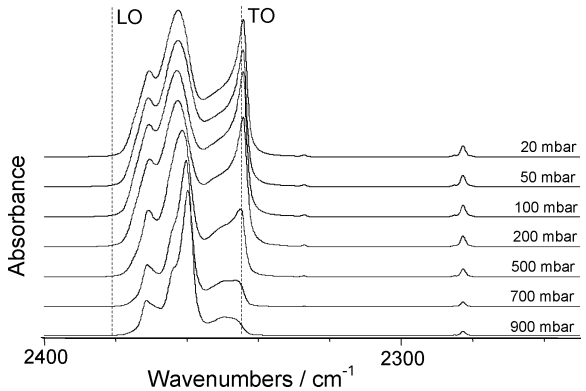

Figure 4. The ν_3-vibration band of CO_2 nanoparticles at 79 K at different buffer-gas pressures. A single pulse of 1002 ppm CO_2 in He was injected into the cell at a buffer-gas pressure between 20 and 900 mbar. Recording started 5 s after pulse injection in each case. The evolution of spectral band structures and band positions indicates a particle shape transformation from cubic-like toward longish particles (or toward particles with longish structures on their surfaces) with decreasing pressure; compare Table 1.

before reaching the inner cooling cell (for results, see Figures 4 and 5). Finally, the different sample gases were separately injected through thinner inlet pipes (for results, see Figures 6 and 7). Using this multiple-tube sample gas inlet technique, the gas components are not mixed before reaching the inner cold area of the cell. In contrast to the continuous inlet, the pulsed injection of the sample gas has the advantage of avoiding gas deposition in the inner inlet tube.

The infrared band intensities of pure H_2O ice (symmetric and antisymmetric O−H stretch mode at 3280 cm^{-1}) and of pure CO_2 ice (antisymmetric C═O stretch mode at 2343 cm^{-1}) are 2.0×10^{-16} and 7.6×10^{-17} cm molec^{-1} (ref 1 and references therein). The CO_2 ice band intensity only varies by about 5% in the temperature interval between 14 and 100 K.[1] We use these band intensities to estimate the mole fractions in binary H_2O/CO_2 nanocomposites.

III. Results and Discussion

A. Carbon Dioxide Nanoparticles. *Particle-Size Estimation.* The average size of the observed particles, shown for example in Figure 2, was estimated by adapting a method presented by Disselkamp and Ewing.[9] If the particles are assumed to have approximately a spherical shape, their average radius can be calculated by comparing the extinction cross section coefficient derived from Mie's theory with the extinction cross section

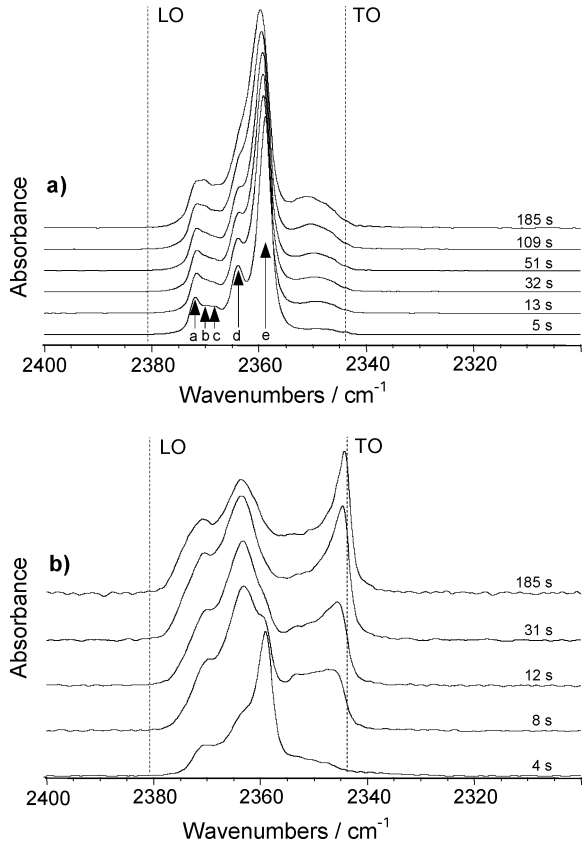

Figure 5. Temporal development of the ν_3-vibration band of CO_2 nanoparticles *x* seconds after one single pulse-injection of 1002 ppm CO_2 in He at a buffer-gas pressure of 900 mbar (series a) and 3 mbar (series b) at 81 K each. For the arrows a−e in series a, see text and Table 2. Note that the shape evolution within 185 s toward longish particles only takes place at low buffer-gas pressures.

coefficient determined from the spectral data. For a numerical calculation of the particle radius, we applied a source code published by Bohren and Huffman.[16] We used no additional optical equipment and extracted the scattering data from the spectra at 5000 cm^{-1}.

In Figure 3, the estimated cluster sizes are shown in relation to the sampling conditions of Figure 2. These particles can be assumed to be approximately spherical (compare next section). It is obvious that the particle size correlates and increases with the sample-gas pressure. The sizes range from about 300 nm at a sample gas pressure of 900 mbar to about 100 nm at 50 mbar. Particles formed at sample gas pressures below 50 mbar should be even smaller. Their size could not be calculated by this method due to the insignificantly small slope of the baseline and the low signal-to-noise ratio at 5000 cm^{-1}.

The CO_2 nanoparticles that show spectra with the typical TO-mode "hook" feature at 2344 cm^{-1} (Figures 4, 5b, 6c, and 7b,d) were estimated to have a size in the range of 50−100 nm with roughly 10^7-10^8 molecules per particle.[11,17]

Particle-Shape and Structure. Meanwhile, it is well known for CO_2 (and N_2O) that the shape of the nanoparticles has a considerable influence on the intense vibration bands of the infrared spectra. The vibrational exciton approach,[9,18−20] which recently has been extended to bigger particles ($n > 1000$) by Signorell et al.,[13,15] has essentially contributed to the assignment of particle-shape and spectral structure. While the absorption intensity of the strongest vibrational bands for crystalline CO_2 (and N_2O) nanoparticles is distributed between the transverse optical (TO) and the longitudinal optical (LO) modes for different particle shapes,[16] the absorption range is extended to the red side (beyond the TO mode) for the amorphous (disordered) state of spheroidal particles[11,17,21] and films.[22,23] In Table 1, band positions and shapes of the ν_3-vibration of the most important particle shapes as slab, sphere, cube, and needle are compiled as a basis for discussion of the measured spectra of Figures 3−7.

Influence of Buffer-Gas Pressure. We start the discussion of the spectroscopic results with the demonstration of the buffer-gas pressure influence on the CO_2 nanoparticle ν_3-vibration band. In a first experiment, 91 ppm CO_2 in helium was filled into the empty cell at 83 K up to a total pressure of 10−900 mbar; see Figure 2. The particle size increases with the filling pressure from below 100 nm (lower trace) up to more than 300 nm (upper trace); compare Figure 3. The spectral shape and band positions indicate that the particles have a spheroidal shape (lower trace) and change toward a cubic shape with edges and corners (upper trace) with higher filling pressures; compare Table 1 and references therein, especially ref 15. The spectra of Figure 2 are in correspondence with spectra of CO_2 nanoparticles generated by pulse-injection at similar temperatures (compare Figure 5 in ref 12).

In a second experiment, only one single pulse of 1002 ppm CO_2 in He was injected into the cell, prefilled with helium buffer gas at a pressure between 900 and 20 mbar, see Figure 4. The main result is that the sideband increases strongly with decreasing buffer-gas pressure exactly at the TO mode wavenumber. Here, the interpretation is clear: at 900 mbar, the spectrum is dominated by one main peak at 2360 cm^{-1} with shoulders in accordance with a cubic-like particle shape. At 200−20 mbar, the spectra evolve toward a two-peak structure with positions at 2344 and 2363 cm^{-1}, which exactly meet the conditions for longish particles as needles or columns, see Table 1.

Temporal Evolution. Further investigations were carried out with respect to the temporal development of the CO_2 nanoparticles inside the cooling cell after injection of one single sample-gas pulse at various buffer-gas pressures. Two selected spectra series for a high and a low buffer-gas pressure at 900 and 3 mbar are depicted in Figure 5. A profile analysis of the first spectrum of Figure 5a shows at least five different peaks at wavenumbers being in good agreement with results of Barnes et al.;[24] compare Table 2.

A noticeable result of Figure 5b is that the sidebands evolve strongly in the course of 100 s. Especially the TO mode band at 2344 cm^{-1} increases at 3 mbar in addition to a blue-shift of the main band position by 5 wavenumbers, whereas at 900 mbar only a minor evolution of the spectra can be observed. A possible interpretation is that the particles evolve from cubic to needle shapes (or toward those particles with needlelike structures on their surfaces) at the low buffer-gas pressure (Figure 5b), but remain at the cubic structure at the higher pressure (Figure 5a). This behavior corresponds with the temporal evolution of the infrared absorption spectra of N_2O nanoparticles generated under similar conditions.[11,17] Furthermore, it is remarkable that the temporal behavior of the spectra shown in Figure 5b is very similar to the pressure dependence of the spectra in Figure 4. It seems that at higher buffer-gas pressures the particles are increasingly inhibited from changing their structure.

B. Composite Water-Ice/Carbon Dioxide Nanoparticles. Composite H_2O/CO_2 nanoparticles were formed by use of different sample-gas inlet techniques. Apart from the OH-dangling bands, which are depicted in Table 3, the CO_2 component has only marginal influence on the water parts of

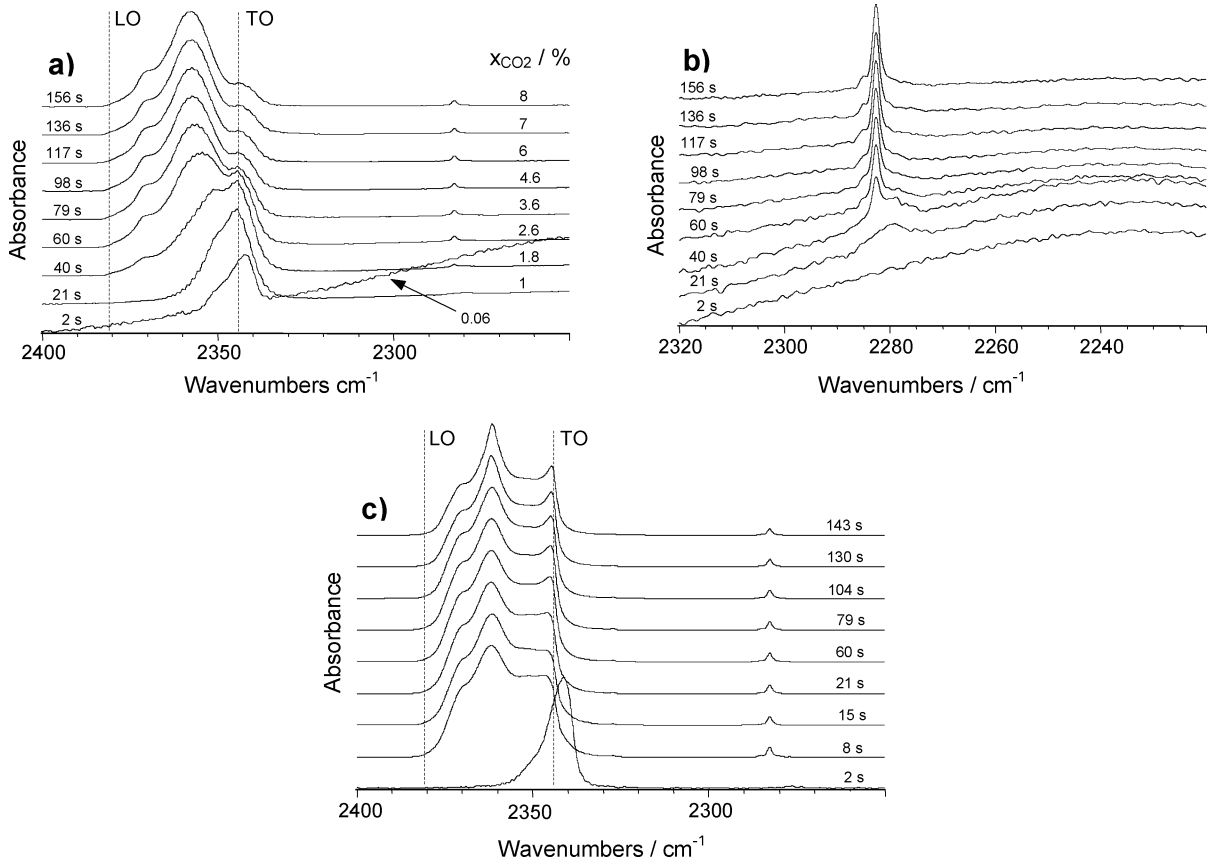

Figure 6. Temporal development of the ν_3-vibration band of composite H_2O/CO_2 nanoparticles during repetitive injection of 11 ppm CO_2 in He (series a) and 1002 ppm CO_2 in He (series c) into water-ice aerosol at 200 mbar and 82 K. The mole fraction x_{CO_2} increases with time from 0.06% to 8% (series a) and from 0.8%, 34%, ..., to 92% (series c). Series b focuses on the ν_3-vibration of the $^{13}CO_2$ isotopomers in the H_2O/CO_2 nanoparticles of series a.

the infrared spectra. The water ice spectra are not shown in the present work.

In a first experiment, the cooling cell was prefilled up to 200 mbar with a water/helium mixture containing 100 ppm H_2O. To the water-nanoparticle aerosol that had been formed by homogeneous nucleation in this way at 81 K, further sample gas mixtures of 11 ppm CO_2 in helium (Figure 6a,b) and 1002 ppm CO_2 in helium (Figure 6c) were pulse-injected every 10 s, 15 times in total in each case. So the ratio of CO_2 to H_2O molecules in the cell increased with time up to a CO_2 mole fraction of about 8% (Figure 6a,b) and up to about 90% (Figure 6c). In Figure 6a and c, the temporal development of the ν_3-band of $^{12}CO_2$ is shown. In both cases, the first trace at 2 s after the first CO_2 injection clearly shows the triangle band shape of amorphous films extending with the steeper edge beyond the TO mode wavenumber;[22,23] also compare Table 1. That means the CO_2 monomers aggregate on the surface of the suspended primary water particles and form part of a disordered film. In the course of further CO_2 injection and subsequent further CO_2 adsorption on the particles, the band shape and band position evolve toward different final spectra.

At the low CO_2 sample gas concentration (Figure 6a,b), the final band shape and position corresponds to a crystalline sphere. This conclusion is supported by the corresponding band evolution of the $^{13}CO_2$ molecules (which have no dipole−dipole coupling with $^{12}CO_2$ neighbors, only about 13% of the $^{13}CO_2$ molecules have equal neighbors and therefore show resonant coupling[9]); see Figure 6b. Here, the second and third trace at 21 and 40 s show very large bandwidths (fwhm, full width at half-maximum) of about 10 cm^{-1} caused by a disordered structure. After approximately 80 s, the bandwidth decreases to about 2 cm^{-1} and the transition to the typical invariant crystalline structure[9] is almost completed. We assume that the CO_2 molecules cover only a (small) part of the water particles. This assumption is supported by the fact that no considerable shift or broadening of the dangling-OH band of the corresponding water spectrum has been observed; compare Table 3. Otherwise, that would be the case because adsorbates as N_2 or CO_2 on water ice surfaces cause a red-shift of the dangling-OH band by more than 20 cm^{-1} and increase the bandwidths by several tens percent,[25,26] as compared to a band position at 3699 cm^{-1} and a bandwidth of about 12 cm^{-1} for bare water nanoparticles.[27]

The situation changes at higher CO_2 sample gas concentrations (Figure 6c). Here, the ν_3-band evolves toward a band shape of crystalline needlelike nanoparticles as discussed above. In contrast to the spectra of Figure 6a, the TO mode feature at 2344 cm^{-1} occurs. Furthermore, in the corresponding water spectra, an additional broader red-shifted OH-dangling band occurs at 3661 cm^{-1} with increasing CO_2 mole fraction in the aerosol. It reaches the same integrated absorbance as the "regular" OH-dangling band at 3699 cm^{-1} after about 50 s. The latter band disappears in the course of further CO_2 injection, and the red-shifted OH-dangling band evolves; compare Table 3. Our interpretation is that, as compared to Figure 6a, here the higher amount of CO_2 molecules is sufficient to cover the whole surface of the suspended primary water particles. Note that the $^{12}CO_2$ molecules obviously form no regular shell around the H_2O cores as they do in the case of $^{13}CO_2$ cores.[7] We do not observe the LO mode band in addition to the TO mode feature, which otherwise should complement the tub structure of hollow spheres; compare Table 1.

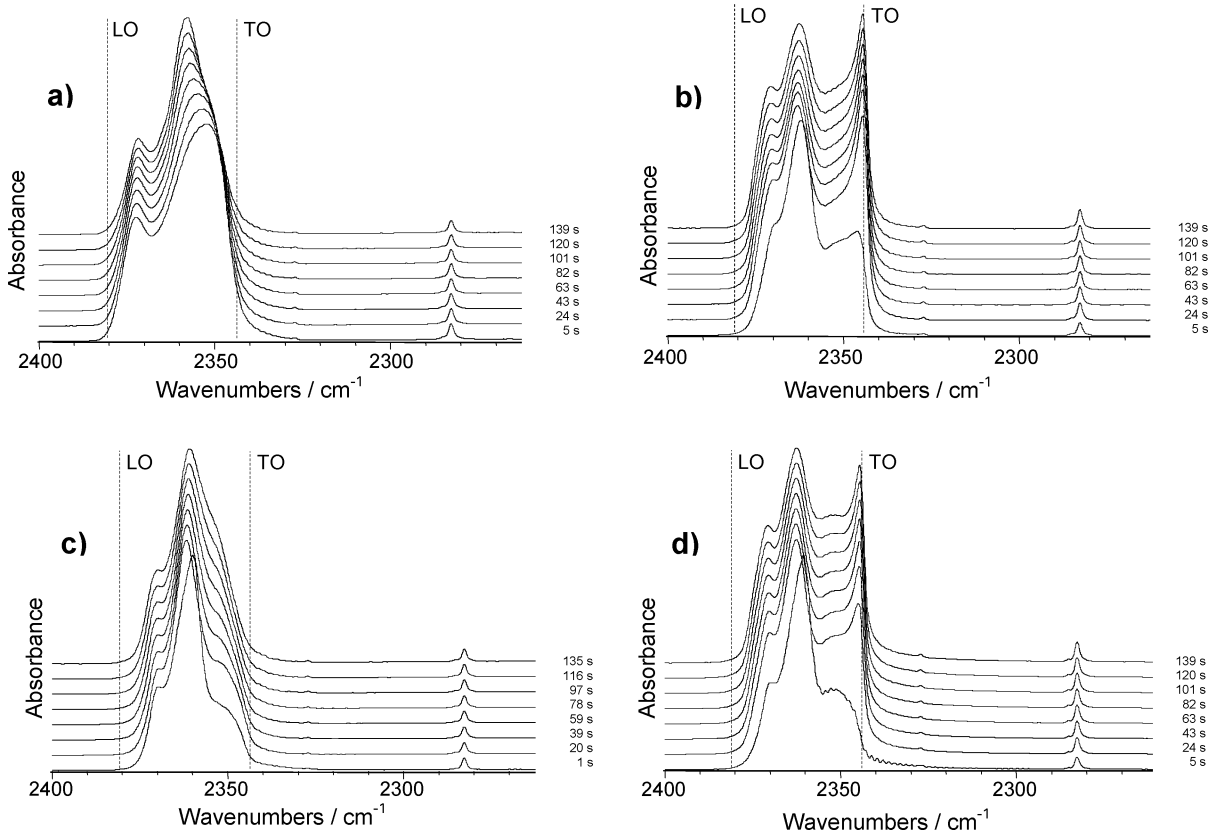

Figure 7. Temporal development of the ν_3-vibration band of H_2O/CO_2 composite and bare CO_2 nanoparticles at 80 K with 100 mbar He buffer-gas pressure. The multiple-tube inlet technique was used. Series a: one pulse-injection of 1% H_2O in He and 0.5 s later one pulse-injection of 1002 ppm CO_2 in He. Series c: one pulse-injection of 1002 ppm CO_2 in He and 0.5 s later one pulse-injection of 1% H_2O in He (reversed injection order). Series b: one pulse-injection of pure He and 0.5 s later one pulse-injection of 1002 ppm CO_2 in He (control experiment for series a). Series d: one pulse-injection of 1002 ppm CO_2 in He and 0.5 s later one pulse-injection of pure He (control experiment for series c).

TABLE 1: Shape and Position of the ν_3-Vibration Band of CO_2 (and N_2O) Nanoparticles in the Size Range of $d = 10-200$ nm, Dependent on Particle Structure and Shape[a]

structure, shape	band-maxima positions	band shape, qualitatively	refs
	Crystalline		
film, disk, slab[b]	$x = \omega_{TO}$	Gaussian	9, 16, 22, 23
film, disk, slab	$x_1 = \omega_{TO}$, $x_2 = \omega_{LO}$	two Gaussians	9, 16, 22, 23
hollow sphere, shell	$x_1 = \omega_{TO}$, $x_2 = \omega_{LO}$	tub, two Gaussians	7, 32
sphere	$x = (2\omega_{TO} + \omega_{LO})/3$	Gaussian	15, 16, 20, 23, 33
sphere with $d = 2$ nm	$x = (2\omega_{TO} + \omega_{LO})/3$	Gaussian, sideband structures	34
sphere with $d = 1000$ nm		broader, red-shifted Gaussian with sideband structures	34
cube	$\omega_{TO} < x < (2\omega_{TO} + \omega_{LO})/3$	Gaussian with substructures at the blue side	9, 15, 16, 33
needle, rod, column	$x_1 = \omega_{TO}$, $x_2 = (\omega_{TO} + \omega_{LO})/2$	two Gaussians	16, 23, 33
	Amorphous		
film, slab	$x < \omega_{TO}$	triangle with the steeper edge at the red side	22, 23
sphere	$\omega_{TO} < x < \omega_{LO}$	broad Gaussian	11, 17, 21

[a] Transverse and longitudinal optical modes of the CO_2 crystal are[20,23,31] $\omega_{TO} = 2344$ cm^{-1} and $\omega_{LO} = 2381$ cm^{-1}, and $(2\omega_{TO} + \omega_{LO})/3 = 2356.3$ cm^{-1} and $(\omega_{TO} + \omega_{LO})/2 = 2362.5$ cm^{-1} for CO_2 nanoparticles. [b] Sample oriented perpendicular to the light beam.

TABLE 2: Absorption Frequencies of ν_3-Vibration Band Substructures of CO_2 Nanoparticles Generated under the Conditions of Figure 5a, in cm^{-1}

this work (Figure 5a)	2372.0	2369.6	2367.7	2363.5	2358.7	
Barnes et al.[24]	2372.1	2369.8	2367.5	2364.4	2360.0	2342.9

Figure 7 describes the experiments using the multiple-tube sample-gas inlet-technique at 80 K. Series a and c show the temporal evolution of the ν_3-vibration of binary H_2O/CO_2 and CO_2/H_2O nanoparticles over 140 s. A single pulse-injection of 1% H_2O in He has been followed 0.5 s later by a further pulse-injection of 1002 ppm CO_2 in He and vice versa. In any case, water is the major component in the system. We suppose homogeneous nucleation of the first and heterogeneous nucleation of the second injected component.

Series b and d show the spectral results of control experiments in contrast to series a and c. Here, the experimental conditions were the same as in series a and c with the exception that the H_2O pulse injections were replaced by injections of pure He. The spectra series b and d are very similar to the series in Figure 5b and show that the presence of a pure He pulse 0.5 s before or after the CO_2 injection (and thus the heat input of the gas pulse) has only marginal influence on the spectra and therefore on the particle shape and its evolution. The comparison between

TABLE 3: Overview of Positions and Widths (fwhm) of the Dangling-OH Bands of the Binary H_2O/CO_2 Nanoparticles Presented in This Work[a]

figure number, order in series	experimental conditions, schematically	position/width in cm^{-1} of "uncovered" OH band	position/width in cm^{-1} of "covered" OH band
Figure 6a	$H_2O \rightarrow$ little CO_2, CO_2, ...		
first spectrum		3697/12	not visible
last spectrum		3697/12	not visible
Figure 6c	$H_2O \rightarrow$ much CO_2, CO_2, ...		
first spectrum		3699/14	not visible
middle spectrum		3699/14	3661/18
last spectrum		not visible	3661/18
Figure 7a	$H_2O \rightarrow$ little CO_2, time evolution		
first spectrum		3694/12	3665/25
middle spectrum		3694/12	3665/25
last spectrum		3694/12	3665/25
Figure 7c	little $CO_2 \rightarrow H_2O$, time evolution		
first spectrum		3693/12	(3670/−) very weak
middle spectrum		3693/12	(3670/−) very weak
last spectrum		3693/12	(3670/−) very weak

[a] There are two different dangling-OH band positions observed in the infrared spectra at approximately 3665 and 3695 cm^{-1} resulting from surface regions of the particles' water parts being covered or uncovered with CO_2 molecules. The uncertainties of position and width are $<\pm 1$ cm^{-1} and $\pm 5\%$.

the spectra of the binary system and the control experiments clearly indicates the influence of water on the ν_3-band of CO_2 and again gives strong evidence for the formation of binary H_2O/CO_2 particles. In contrast to the control experiments, the presence of water inhibits the development of the TO mode feature at 2344 cm^{-1} in Figure 7a and c.

Dependent on the temporal order of the injected components, series a and c show different "start" spectra. They develop over about 140 s to similar "end" spectra. This indicates a change in particle structure toward a thermodynamically stable state. (In series a, the maximum is blue-shifted from 2353 to 2358 cm^{-1}, and the band's half width (fwhm) decreases from 29 to 23 cm^{-1}. In series c, the maximum is red-shifted from 2362 to 2361 cm^{-1}, and the band's half width increases from 10 to 15 cm^{-1}.)

In the case of series a, there is no indication that the CO_2 molecules form any kind of mantle or hollow sphere around the primary water nuclei. Similar to the results depicted in Figure 6a, a tub structure with two band maxima at the TO and LO mode wavenumbers (compare Table 1) is completely missing. The dangling-OH band gives more quantitative information to the extent of water-particle surface covering by CO_2 molecules; compare Table 3. From the presence of both the regular OH-dangling band at 3694 cm^{-1} and a broader red-shifted OH-dangling band at 3665 cm^{-1}, which show comparable integrated absorbances, it can be deduced that less than 50% of the total water particle surface is covered. It has to be taken into account that adsorbates on the water particle surface increase the integrated absorbance of the OH-dangling band.

In the case of series c, there is only a very weak red-shifted OH-dangling band at 3670 cm^{-1} over the whole time range, in contrast to the regular OH-dangling band; see Table 3. This indicates that the CO_2 molecules seem not to spread on the water particle surfaces and consequently form no shell around it at 80 K. Devlin and Buch classified CO_2 as a "weak" adsorbent that is not able to penetrate ice nanocrystals at cryogenic temperatures in the range of 70−140 K.[28] Therefore, we conclude from our experiments that water and carbon dioxide aggregate in separated phases and form nanocomposites.

IV. Conclusions

In the present study, we have investigated CO_2 and especially binary H_2O/CO_2 nanoparticles at about 80 K in a long-path collisional cooling cell. FTIR spectroscopy was used to study the time-dependence of the carbon dioxide ν_3-vibration band of the particles and composites in the aerosol phase and their temporal evolution. Different sample-gas inlet techniques have been applied. For the pulse-injection technique, the most important parameters to adjust the average particle size are temperature and sample-gas concentration. For the simpler flow-in technique, the particle size showed a root-function dependence on the sample-gas pressure in the cell (Figure 3). Both techniques combined allow us to cover the size range of below 1 to more than 1000 nm for molecular nanoparticles as $(CO_2)_n$ or $(N_2O)_n$; compare refs 11, 12, and 27.

The shape of the investigated CO_2 nanoparticles ranges from globular or cubic-like to apparently longish, needlelike. The particle shape is mainly determined by the buffer-gas pressure and by the progress of the temporal evolution. Both dependences are very similar to those we obtained for N_2O nanoparticles.[11,17] The experimental results concerning spectral band positions and band shapes support the theoretical picture as gained by classic scattering theory, the electrostatic model, or the exciton approach; compare Table 1.

More revealing conclusions can be drawn from the binary H_2O/CO_2 particle spectra presented in Figures 6 and 7. From the spectra of the carbon dioxide ν_3-vibration band and the water OH-dangling band and their temporal behavior, we conclude that the molecules of both components aggregate to composite particles in each case. Otherwise, for example, in Figure 7c, there would remain a significant amount of homogeneously nucleating CO_2 molecules forming pure CO_2 nanoparticles in the cell and at least parts of a TO mode feature should occur in the spectra. This is not the case.

During the condensation process of CO_2 monomers on water nanoparticles, at first, the CO_2 molecules form a disordered (amorphous) slab on parts of the water ice surfaces, probably dominated by the foreign ice-surface structure (Figure 6). After further addition of CO_2 molecules up to a mole fraction of about 4%, the carbon dioxide slabs seem to show increasingly epitaxial growth and evolve toward crystalline globular humps on the water particles. When considerably more CO_2 is added up to a mole fraction of more than 50%, the water particles are completely covered by CO_2 molecules.

In the experiment leading to the spectral series in Figure 7, about 10-fold more H_2O than CO_2 molecules is in the cooling system. Independently of the order of nucleation of the

components, the comparison of the spectral series 7a and 7c indicates that the binary particles evolve toward similar particle structures. Furthermore, we could not observe in any experiment that the CO_2 molecules form regular shells around the water particles as they do around $^{13}CO_2$ cores.[7]

The molecules of the second component use the nanoparticles of the first component as nuclei for condensation, but the nanocomposites do not show a significant tendency to form mixed crystals at 80 K. They rather stick together in separated regions of the binary aggregates. These conclusions are supported by semiempirical AM 1 calculations we carried out with the Mopac module[29] for small H_2O/CO_2 systems at 80 K. First results show that the CO_2 molecules are forced to move from inside to the surface of the cluster, certainly caused by the stronger H-bonding forces of water. The calculations should be intensified in the future. Our observations are in accordance with the picture of interstellar ice grains of H_2O, CO, and CO_2, which usually appear in polar and nonpolar phases.[1,30]

Acknowledgment. We thank W. Lahmann for fruitful discussions.

References and Notes

(1) Gerakines, P. A.; Schutte, W. A.; Greenberg, J. M.; van Dishoeck, E. F. *Astron. Astrophys.* **1995**, *296*, 810.
(2) Block, P. A.; Marshall, M. D.; Pedersen, L. G.; Miller, R. E. *J. Chem. Phys.* **1992**, *96*, 7321.
(3) Sadlej, J.; Makarewicz, J.; Chalasinki, G. *J. Chem. Phys.* **1998**, *109*, 3919.
(4) Fleyfel, F.; Devlin, J. P. *J. Phys. Chem.* **1988**, *92*, 631.
(5) Fleyfel, F.; Devlin, J. P. *J. Phys. Chem.* **1991**, *95*, 3811.
(6) Hernandez, J.; Uras, N.; Devlin, J. P. *J. Phys. Chem. B* **1998**, *102*, 4526.
(7) Bauerecker, S. *Phys. Rev. Lett.* **2005**, *94*, 033404.
(8) Fleyfel, F.; Devlin, J. P. *J. Phys. Chem.* **1989**, *93*, 7292.
(9) Disselkamp, R.; Ewing, G. E. *J. Chem. Phys.* **1993**, *99*, 2439.
(10) Gough, T. E.; Wang, T. *J. Chem. Phys.* **1995**, *102*, 3932.
(11) Kunzmann, M. K.; Signorell, R.; Taraschewski, M.; Bauerecker, S. *Phys. Chem. Chem. Phys.* **2001**, *3*, 3742.
(12) Bauerecker, S.; Taraschewski, M.; Weitkamp, C.; Cammenga, H. K. *Rev. Sci. Instrum.* **2001**, *72*, 3946.
(13) Signorell, R. *J. Chem. Phys.* **2003**, *118*, 2707.
(14) Bonnamy, A.; Georges, R.; Benidar, A.; Boissoles, J.; Canosa, A.; Rowe, B. R. *J. Chem. Phys.* **2003**, *118*, 3612.
(15) Signorell, R.; Kunzmann, M. K. *Chem. Phys. Lett.* **2003**, *371*, 260.
(16) Bohren, C. F.; Huffman, D. R. *Absorption and scattering of light by small particles*; John Wiley & Sons: New York, 1983.
(17) Kunzmann, M. K.; Bauerecker, S.; Suhm, M. A.; Signorell, R. *Spectrochim. Acta, Part A* **2003**, *59*, 2855.
(18) Cardini, G.; Schettino, V.; Klein, M. L. *J. Chem. Phys.* **1989**, *90*, 4441.
(19) Disselkamp, R.; Ewing, G. E. *J. Chem. Soc. Faraday Trans.* **1990**, *86*, 2369.
(20) Ovchinnikov, M. A.; Wight, C. A. *J. Chem. Phys*. **1994**, *100*, 972.
(21) Bauerecker, S., unpublished results.
(22) Falk, M.; Seto, P. F. *Can. J. Spectrosc.* **1986**, *31*, 134.
(23) Ovchinnikov, M. A.; Wight, C. A. *J. Chem. Phys*. **1993**, *99*, 3374.
(24) Barnes, J. A.; Gough, T. E.; Stoer, M. *J. Chem. Phys.* **1991**, *95*, 4840.
(25) Rowland, B.; Fisher, M.; Devlin, J. P. *J. Chem. Phys.* **1991**, *95*, 1378.
(26) Devlin, J. P.; Silva, S. C.; Rowland, B.; Buch, V. In *Hydrogen Band Networks*; Bellissent-Funel, M. C., Dore, L. C., Eds.; Kluwer: Amsterdam, 1994.
(27) Buch, V.; Bauerecker, S.; Devlin, J. P.; Buck, U.; Kazimirski, J. K. *Int. Rev. Phys. Chem.* **2004**, *23*, 375.
(28) Devlin, J. P.; Buch, V. *J. Phys. Chem. B* **1997**, *101*, 6095.
(29) *ChemBats3D pro*; CambridgeSoft Corp., 1999; http://www.camsoft.com.
(30) Greenberg, J. M.; van de Bult, C. E. P. M.; Allamandola, L. J. *J. Phys. Chem.* **1983**, *87*, 4243.
(31) Decius, J. C.; Hexter, R. M. *Molecular Vibrations in Crystals*; MGraw-Hill: New York, 1977.
(32) Buch, V.; Delzeit, L.; Blackledge, C.; Devlin, J. P. *J. Phys. Chem.* **1996**, *100*, 3732.
(33) Kunzmann, M. K. Doctoral Thesis, Cuvillier Verlag, Göttingen, 2002.
(34) Signorell, R. *Mol. Phys.* **2003**, *101*, 3385.
(35) Torchet, G.; Bouchier, H.; Farges, J.; de Feraudy, M.-F.; Raoult, B. *J. Chem. Phys.* **1984**, *81*, 2137.
(36) Bartell, L. S. *Chem. Rev.* **1986**, *86*, 491.
(37) Gough, T. E.; Wang, T. *J. Chem. Phys.* **1996**, *105*, 4899.
(38) Torchet, G.; de Feraudy, M.-F.; Boutin, A.; Fuchs, A. H. *J. Chem. Phys.* **1996**, *105*, 3671.